INTERNATIONAL JOURNAL OF MICROWAVE AND OPTICAL TECHNOLOGY

VOL. 3, NO.3 , JULY 2008

Finite-Volume Time-Domain Method for Electromagnetic Modelling: Strengths, Limitations and Challenges

C. Fumeaux*, D. Baumann**, G. Almpanis***, E.P. Li** and R. Vahldieck***

* School of Electrical and Electronic Engineering
The University of Adelaide, Adelaide, South Australia 5005
Tel: +61 8830 35667; Fax: +61 8303 4360; E-mail: cfumeaux@eleceng.adelaide.edu.au

** Computational Electromagnetics and Electronics, Institute of High Performance Computing
A*STAR, Singapore 117528
Tel: +65 6419 1594; Fax: +65 6419 1380; E-mail: dirk@ihpc.a-star.edu.sg

*** Laboratory for Electromagnetic Field Theory and Microwave Electronics
ETH Zurich, Zurich, CH-8092, Switzerland
Tel: +41 44 632 0601; Fax: +41 44 632 1647; E-mail: almpanis@ifh.ee.ethz.ch

***Abstract*- The attractive features of the Finite-Volume Time-Domain (FVTD) method for the solution of Maxwell's equations come from the application in unstructured polyhedral meshes combined with an explicit time stepping. This paper reviews current developments of the FVTD method and provides an assessment of its potential as a general-purpose electromagnetic simulation technique. A tutorial on the FVTD algorithm is given first, followed by a discussion of the strengths as well as of the limitations of the method. More generally, the challenges associated with a widespread use of conformal time-domain techniques are described. The addressed points are illustrated by a representative application of the method, which involves the detailed modelling of dielectric resonator antennas (DRAs) in several configurations.**

***Index Terms*- Time-domain analysis, Finite-Volume Time-Domain method (FVTD), dielectric resonator antenna (DRA).**

I. INTRODUCTION

The development of novel methods for electromagnetic (EM) simulations is motivated by the increasing need for numerical analysis tools, which are able to handle complex multi-scale structures. In the class of methods based on a volume discretization of space, the Finite-Difference Time-Domain (FDTD) method dominates the modelling of EM problems since many years. Numerous attempts have been made to circumvent the constraint of the original FDTD Yee scheme to structured Cartesian grids: In particular, various conformal approaches that locally alter the FDTD algorithm near curved or slanted surfaces have been proposed, as well as sub-gridding techniques that allow accommodating various scales of structural sizes (see, e.g. [1]). Besides those efforts, alternatives have been sought in time-domain techniques applied completely in unstructured meshes. This second approach presents the conceptual advantage of requiring no local algorithm alterations to handle non-Cartesian surfaces and small details, and thus reduces high-complexity problems to the meshing process. This has lead at the very end of the 1980's to the first Maxwell solver based on the Finite-Volume Time-Domain (FVTD) method [2],[3], which advantageously combines an explicit time stepping with an unstructured space discretization.

The present paper first provides an introduction to the FVTD algorithm in Sec. II, emphasizing on the physical interpretation rather than on the mathematical formulation. It then describes in Sec. III the strengths as well as the limitations of the algorithm for EM simulations. The discussion

INTERNATIONAL JOURNAL OF MICROWAVE AND OPTICAL TECHNOLOGY

VOL. 3, NO.3 , JULY 2008

identifies challenges lying ahead for a widespread efficient application of the method. In Sec. IV, practical simulations illustrate the points discussed. The examples consider the simulation of different configurations of probe-fed dielectric resonator antennas (DRAs).

II. FVTD Tutorial

The finite-volume formulation of Maxwell's equations is inspired from computational fluid dynamics. It is based on the Maxwell's curl equations expressed in their conservative form [4] with the condensed notation

$$\alpha \frac{\partial \boldsymbol{U}}{\partial t} + \mathrm{Div}\boldsymbol{F}(\boldsymbol{U}) = 0 \,. \tag{1}$$

In this equation, the six-component vector $\boldsymbol{U}$ contains all the $\boldsymbol{E}$ and $\boldsymbol{H}$ field components, i.e. $\boldsymbol{U} = (E_x, E_{y,} E_z, H_x, H_{y,} H_z)^T$. The 6×6 matrix α describes the material parameters. Assuming an isotropic media, this matrix becomes a diagonal matrix filled with the permittivity ε (three first diagonal elements) and permeability μ (three last diagonal elements). The function $\boldsymbol{F}(\boldsymbol{U}) = \left(F_1(\boldsymbol{U}), F_2(\boldsymbol{U}), F_3(\boldsymbol{U})\right)$ is constructed as

$$\begin{aligned} F_1(\boldsymbol{U}) &= (0, H_z, -H_y, 0, -E_z, E_y)^T \\ F_2(\boldsymbol{U}) &= (-H_z, 0, H_{x,}, E_z, 0, -E_x)^T \\ F_3(\boldsymbol{U}) &= (H_{y,}, -H_x, 0, -E_y, E_x, 0)^T \end{aligned} \,. \tag{2}$$

and the divergence operator Div is applied on each row of $\boldsymbol{F}(\boldsymbol{U})$ according to

$$\mathrm{Div}\boldsymbol{F}(\boldsymbol{U}) = \frac{\partial F_1(\boldsymbol{U})}{\partial x} + \frac{\partial F_2(\boldsymbol{U})}{\partial y} + \frac{\partial F_3(\boldsymbol{U})}{\partial z} \,. \tag{3}$$

It is straightforward to demonstrate that, in (1), the curl terms in Maxwell's equations are reconstructed by applying this divergence operation (3) on the function $\boldsymbol{F}(\boldsymbol{U})$ defined in (2). To obtain the finite-volume formulation, the conservative representation (1) of the Maxwell's system is integrated over a volume V, and the Gauss theorem is applied subsequently on the divergence term. This yields the finite-volume fundamental equations [5]

$$\begin{aligned} \frac{\partial}{\partial t}\iiint_V \vec{D}\, dv &= \oiint_{\partial V} \underbrace{\vec{n}\times\vec{H}}_{-\vec{\Phi}^H} da \\ -\frac{\partial}{\partial t}\iiint_V \vec{B}\, dv &= \oiint_{\partial V} \underbrace{\vec{n}\times\vec{E}}_{\vec{\Phi}^E} da \,, \end{aligned} \tag{4}$$

which relates volume integrals on the left-hand side to surface integrals on the right-hand side. A physical interpretation of (4) derived from fluid dynamics considers variations of conserved quantities in the volume V that are compensated by fluxes $\vec{\Phi}^H$ and $\vec{\Phi}^E$ through the volume boundary ∂V. Those mathematically defined fluxes can be expressed as the vector product of the outward-pointing normal vector $\vec{n}$ with the field vectors ($\vec{H}$ or $\vec{E}$), and therefore, are completely determined by the tangential field components on the boundary surface of the cells.

For numerical implementation of (4), the full computational space has to be partitioned in a polyhedral mesh. For practical computations, a tetrahedral mesh appears attractive, because it offers accurate geometrical resolution of complex structures and can be created using widely available good-quality mesh generators. Considering an elementary tetrahedral cell with volume V_i and homogeneous material properties ε_i and μ_i, the system (4) can be expressed in the semi-discrete form as

$$\begin{aligned} \varepsilon_i V_i \frac{\partial}{\partial t}\vec{E}_i &= \sum_{k=1}^{4} \underbrace{\left(\vec{n}_k \times \vec{H}_k\right)}_{-\vec{\Phi}_k^H} F_k \\ -\mu_i V_i \frac{\partial}{\partial t}\vec{H}_i &= \sum_{k=1}^{4} \underbrace{\left(\vec{n}_k \times \vec{E}_k\right)}_{\vec{\Phi}_k^E} F_k \,, \end{aligned} \tag{5}$$

where the fluxes are summed over the 4 triangular cell faces with area F_k and outward pointing vector $\vec{n}_k$, with $k = 1,...,4$. In the system (5), the field vectors $\vec{E}_i$ and $\vec{H}_i$

associated to the considered cell i represent averages integrated over the cell volume. Correspondingly, the vectors $\vec{E}_k$ and $\vec{H}_k$, which are required to compute the fluxes $\vec{\Phi}_k^H$ and $\vec{\Phi}_k^E$, are averaged over the cell faces. The error in the computed solution of (5) is introduced through inaccurate numerical computation of these averaged values.

Several possible implementations of the finite-volume algorithm exist, and a fundamental classification can be provided by the way the field variables are located at a fixed given point in the elementary cells (finite volumes). The electric and magnetic fields can be collocated or staggered, in either a cell-centred or node-based arrangement. The most common FVTD implementations consider cell-centred collocated configurations, i.e. with both the unknown field vectors $\vec{E}_i$ and $\vec{H}_i$ placed in the barycentre of the cell i. The auxiliary values $\vec{E}_k$ and $\vec{H}_k$ required at the cell boundaries are correspondingly located in the face centres, as suggested in Fig. 1(a). Inside this framework, several scheme variations exist, depending on how the integrations are carried out. A commonly employed scheme is described in the following.

A critical aspect of the FVTD algorithm lies in the accurate determination of the field vectors on the face centres based on barycentric field values. For this purpose, the monotonic upwind scheme for conservation laws (MUSCL) [6] uses a linear function constructed from the barycentre field values and the field gradients estimated in the barycentre. This can be written as

$$\begin{aligned} \vec{E}_k &= \vec{E}_i + \nabla\vec{E}_i \cdot \overrightarrow{dl}_{ik} \\ \vec{H}_k &= \vec{H}_i + \nabla\vec{H}_i \cdot \overrightarrow{dl}_{ik} \ , \end{aligned} \tag{6}$$

where the vector $\overrightarrow{dl}_{ik}$ represents the vector from the barycentre to the face centre , as illustrated in Fig. 1(b) (where for clarity, only the magnetic field for one face is represented). The numerical evaluation of the gradient can be obtained from field values in the cells adjacent to the considered cell, as described in detail in [4].

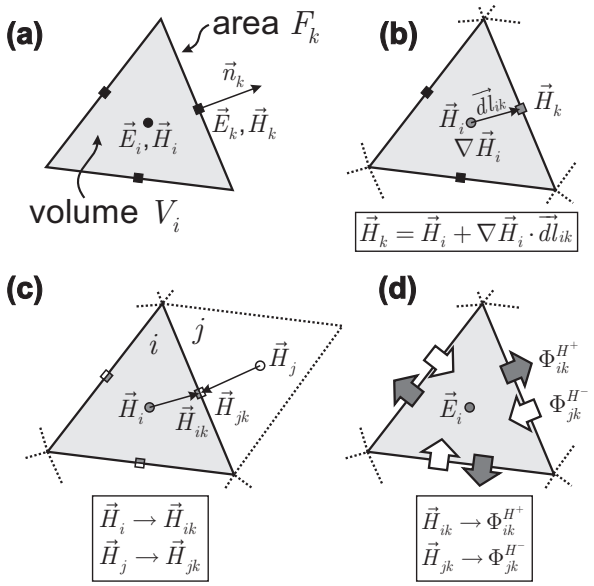

Fig. 1. Two-dimensional representation of a FVTD cell. (a) Geometry and location of the unknowns, (b) MUSCL for the face-centre field vectors. (c) Two-sided computation of the face-centre field vectors. (d) Flux-splitting algorithm illustrating the interaction of cell *i* with neighbour cells.

If the triangular face that forms the boundary between the two tetrahedral cells i and j is considered (as shown in Fig. 1(c)), there are obviously two distinct approximations of the face centre fields that can be obtained, depending on the side where the upwind scheme (MUSCL) is applied. The resulting field vectors are denoted as $\vec{E}_{ik}, \vec{H}_{ik}$ and $\vec{E}_{jk}, \vec{H}_{jk}$, and they provide the basis to compute the fluxes that describe the interaction between adjacent cells. A robust implementation of this interaction is provided by the flux-splitting algorithm, which is based on characteristic theory and separates the fluxes through the face k into the outgoing and incoming contributions [3]

$$\begin{aligned} \vec{\Phi}_k^H &= \vec{\Phi}_{ik}^{H^+} + \vec{\Phi}_{jk}^{H^-} \\ \vec{\Phi}_k^E &= \vec{\Phi}_{ik}^{E^+} + \vec{\Phi}_{jk}^{E^-} \ , \end{aligned} \tag{7}$$

INTERNATIONAL JOURNAL OF MICROWAVE AND OPTICAL TECHNOLOGY

VOL. 3, NO.3 , JULY 2008

with the following notation and interpretation (Fig. 1(d))

- The outgoing fluxes are denoted as $\vec{\Phi}_{ik}^{H^+}$ and $\vec{\Phi}_{ik}^{E^+}$. The subscript i indicates that they are computed on the basis of $\vec{H}_{ik}, \vec{E}_{ik}$, i.e. that they originate from the considered cell i.
- The incoming fluxes are denoted as $\vec{\Phi}_{jk}^{H^-}$ and $\vec{\Phi}_{jk}^{E^-}$. The subscript j indicates that they are computed on the basis of $\vec{H}_{jk}, \vec{E}_{jk}$, i.e. that they originate from the adjacent cell j.

The actual principle of the flux splitting relies on the separation of waves propagating along the direction of the normal vector $\vec{n}_k$ according to the sign of their eigenvalues. An explicit matrix formulation of the split fluxes can be found, e.g. in [4],[7]. The final semi-discrete equation for the field vector in cell i can be expressed in compact notation as

$$\alpha \frac{\partial \boldsymbol{U}_i}{\partial t} V_i = -\sum_{k=1}^{4} \left[\underbrace{\tilde{A}(\vec{\boldsymbol{n}}_k)^+ \boldsymbol{U}_{ik}}_{\boldsymbol{\Phi}_{ik}^+} + \underbrace{\tilde{A}(\vec{\boldsymbol{n}}_k)^- \boldsymbol{U}_{jk}}_{\boldsymbol{\Phi}_{jk}^-} \right] F_k \tag{8}$$

where $\tilde{A}(\vec{\boldsymbol{n}}_k)^{+/-}$ are 6×6 matrices that describe the separated fluxes (+ for outgoing flux, and – for incoming flux) for the face *k* with normal vector $\vec{\boldsymbol{n}}_k$.

In the FVTD framework, the flux-splitting algorithm can be exploited to implement conveniently the following features:

- Port implementation: The excitation of an active port can be added to the incoming fluxes $\boldsymbol{\Phi}_{jk}^-$ on the faces that build the port. The tangential field distribution of the excited mode needs to be known. Furthermore, the split fluxes can be uniquely related to the incident and reflected waves, allowing a convenient S-parameter extraction [7].
- Absorbing boundary condition (ABC): The Silver-Müller ABC is implemented by setting incoming fluxes at the truncating boundary to zero, i.e. $\boldsymbol{\Phi}_{jk}^- = 0$. This first-order ABC is computationally extremely inexpensive, however only exact for normal incidence.

The combination of MUSCL with the flux-splitting algorithm yields a solution of the semi-discrete formulation (8) with second-order accuracy in space. To obtain an explicit formulation, a time-discretization is introduced. This can be achieved using standard iteration techniques such as, e.g. the second-order Runge-Kutta method. The implementation presented here makes use of a second-order Lax-Wendroff predictor-corrector time discretization [4].

III. STRENGTHS AND LIMITATIONS

Since its introduction as electromagnetic simulation technique, the FVTD method has been traditionally applied in scattering problems (e.g. [3],[8]) and increasingly thereafter in antenna and microwave engineering problems (e.g. [9-12]). This has revealed the strengths of this method, but also – as for any numerical method – disclosed some limitations.

A. Strengths

The properties of the FVTD method that make it attractive for a broad range of electromagnetic problems come from the explicit time-domain treatment and from the geometrical flexibility of the implementation in unstructured polyhedral meshes. In fact, it is the combination of these two features that make the specificity of FVTD and motivate research efforts on the method.

For numerous engineering applications, time-domain analysis is attractive, as it is particularly suited to the modelling of broadband and transient phenomena. Further, an explicit time-marching algorithm translates into a linear memory increase with the number of cells, and is amenable to be parallelized [13]. This appears promising for the solution of problems with an increasing size and/or level of details resolution.

In the perspective of dealing with the growing complexity of electromagnetic problems, the

conformal treatment of boundaries in the FVTD method is a powerful characteristic. As mentioned, this geometrical flexibility is intrinsic to the technique and is a direct benefit of the implementation in an unstructured mesh. The most commonly used irregular mesh types are tetrahedral and hexahedral. In particular, a space discretization consisting of tetrahedrons is very convenient since meshing tools capable of producing high-quality tetrahedral meshes are readily available. Such a volume mesh is built on a triangulation of the boundary surfaces and allows discretizing curved or slanted surfaces accurately, while keeping the number of necessary triangles to a minimum.

In addition, strong variations of cell size (i.e. also of volumes) can be introduced in the mesh to resolve fine details embedded in larger structures. The geometrical resolution of the details can then be achieved by creating locally, i.e. where needed, a fine mesh adapted to the feature size. This inhomogeneity of cell size, which is advantageous for multi-scale problems, does not alter the standard connectivity in the tetrahedral mesh (i.e. each cell has four neighbours), and therefore does not require modification of the FVTD algorithm. Similarly, using an inhomogeneous spatial discretization benefits the treatment of geometries where variations of material properties are present, since the domains with denser media can be discretized with a finer mesh.

The conformal treatment of boundaries can also be exploited to shape the computational domain truncation for open-space radiation and scattering problems. The benefit can be expressed in two ways. Firstly, the outer boundary can be shaped so that radiated waves will impinge onto the ABC at near-normal incidence. For an antenna problem, a spherical boundary around the device allows nearly matching the shape of the phase fronts, provided a sufficient large radius is used. In practice, this allows reducing reflection coefficients down to -40 or -50 dB for a simple Silver-Müller ABC. Secondly and more generally, using a spherical or ellipsoidal truncating boundary permits in many cases a reduction of the total volume of the computational domain, thus decreasing the computational cost (as illustrated below in Sec. IV.C). This is best used in conjunction with finite-volume absorbers of the perfectly-matched layers (PML) type, as demonstrated for a radial configuration in [14].

B. Limitations

Paradoxically, the limitations of the FVTD method are, in fact, also a consequence of the unstructured mesh. They concern mainly two relevant aspects: The computational efficiency and the spatial convergence.

Considering the FVTD formulation (8), it appears clearly that the update of a FVTD tetrahedral cell is computationally costlier in terms of CPU time and memory compared to the update of a FDTD Yee cell. Firstly, as each tetrahedral cell is different from its neighbours, more geometrical information and connectivity need to be stored in the memory (even in the form of aggregated coefficients). Secondly, the unstructured nature of the mesh introduces a certain randomness of memory access, and therefore decreases its efficiency. And thirdly, more operations are needed to update a single FVTD cell than a Yee cell. Therefore, the FVTD method becomes interesting for the simulation of devices, where the unstructured mesh allows an accurate modelling of the geometry using a distinctly smaller number of cells than a regular Cartesian grid would require. This condition is very likely to be fulfilled for the simulation of multi-scale structures.

A second limitation of the method is related to the low-order of the approximation in the FVTD cell. As expressed in (6) the field values on the face centres are retrieved on the basis of barycentre values extrapolated with a linear function. The low order is revealed by mesh-induced noise and numerical dissipation [15] that set requirements on the mesh for a desired

INTERNATIONAL JOURNAL OF MICROWAVE AND OPTICAL TECHNOLOGY

VOL. 3, NO.3 , JULY 2008

simulation accuracy. These requirements can be summarized as follows:

- Mesh fineness: The discretization at the highest frequency of interest is required to be a small fraction of the wavelength in the medium considered. For a coarse discretization of $\lambda/10$, numerical dissipation will be observed in the results and might compromise the accuracy of the results, especially for resonant structures.
- Mesh quality: The quality of a mesh can be quantified by considering, e.g. the longest/shortest edge ratio for each tetrahedron, or its volume to surface ratio. Ideal tetrahedrons are close to regular, whereas flat or skewed tetrahedrons introduce computational errors which are manifested as numerical noise. In extreme cases, even the stability of the computation might be compromised.
- Mesh inhomogeneity: In a tetrahedral mesh, the transition from a finely meshed region (e.g. feed of an antenna) to a coarsely meshed region (e.g. free-space) can be realized over a short distance, while remaining smooth (see e.g. [11]). A fast transition allows lowering the total number of cells. However, a too fast transition is bound to reduce the quality of the mesh and therefore the accuracy of the simulation.

Those empirical requirements on the mesh indicate a compromise between the mesh quality and fineness on one side, and the accuracy of the results on the other side.

C. Future Challenges

The FVTD method has proven to be very attractive for solving complex and multi-scale problems. More generally, a growing need for conformal time-domain computations can be expected for the design and analysis of increasingly complex electromagnetic devices. Therefore, the most important challenges will involve addressing the mentioned limitations of the method.

The first aspect regards the increase of the spatial convergence. Towards this end, higher-order FVTD schemes have been proposed [10],[16]. However, these implementations are based on spatially extended field interpolations around each tetrahedron, and therefore, might not enable an accurate treatment of boundaries. Higher-order methods that are based on a higher-order treatment *in cell*, such as the Discontinuous Galerkin (DG) method (e.g., [17],[18]) appear more promising, and significant efforts have been and are invested in this direction. It must be further noted that many aspects of the discussion presented in this paper are shared by the different conformal time-domain methods.

The second aspect concerns the computational efficiency of conformal time-domain algorithms. Towards an enhancement of the performance, a multi-domain analysis appears essential. A step in this direction has been achieved with the development of local time-stepping algorithms [19][20]. Further, the strategy of using a locally implicit or a hybrid explicit/implicit scheme [21] can further relax the time-step condition for stability when tiny cells are present in a refined mesh. Alternatively, for the class of problems that include multiple objects, an hybridization with integral equations has also been proposed [22]. In the frame-work of higher-order methods, a multi-domain multi-order strategy provides an attractive solution [23].

IV. APPLICATION EXAMPLES: DRAs

To illustrate the application of the FVTD method, simulations of probe-fed DRAs of various shapes and configurations are shown in the following. DRAs consist of a dielectric resonator placed on a ground plane in an open environment. The radiation Q factor of those devices in their low-order resonant modes is low and therefore, they can be used as radiators as first demonstrated by Long et al. in 1983 [24]. Compared to microstrip antennas of comparable complexity, DRAs are characterized by a small size, a high efficiency and a wide bandwidth of operation. In particular,

INTERNATIONAL JOURNAL OF MICROWAVE AND OPTICAL TECHNOLOGY

VOL. 3, NO.3 , JULY 2008

wide bandwidths can be achieved by combining several modes with similar radiation characteristics, at slightly offset resonance frequencies. Optimizing the properties of a DRA can be achieved by looking into the dielectric resonator shape, into the feed design, and/or into the materials involved. In the following, the first two examples concern shape variations around a rectangular shape. The emphasis of the discussion is placed on the simulation of the devices with the FVTD method. The third example considers mutual coupling of DRAs.

A. Two-Step DRA

The first example considers a two-step dielectric structure fed by a simple coaxial probe according to the configuration shown in Fig. 2. The design concept for this antenna has been described previously in [25]. The two-step dielectric resonator can be realized by joining two slabs made of Rogers TMM® 10i laminate, with a relative permittivity $\varepsilon_r = 9.8$. The taller of the two slabs has dimensions $l_1 \times w_1 \times h_1 = 17 \times 3.5 \times 25$ mm^3, the smaller slab is $l_2 \times w_2 \times h_2 = 10 \times 3.5 \times 20$ mm^3. The probe length (9.6 mm) is chosen for best matching.

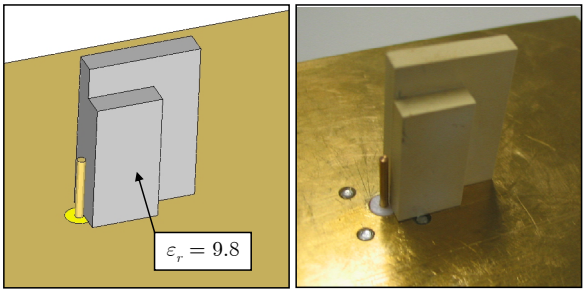

Fig. 2. Geometry of the probe-fed two-step DRA. Left: simulation model, right: fabricated device.

The surface discretization of the device is illustrated in Fig. 3. Three different scales of discretization are shown in the picture. First the ground plane, which is in the air, is discretized with a fraction of the shortest free-space wavelength of interest λ_0. This fraction is typically smaller than 1/10. For example, as depicted in the Fig. 3, a triangulation with $\lambda_0/15$ allows achieving a very good spatial convergence. A second scale of discretization consists in the dielectric resonator itself. Inside the dielectric, the wavelength is shortened by a factor of $\sqrt{\varepsilon_r}$ and consequently requires a correspondingly finer discretization (in the present case by a factor around three). Finally, near the feeding coax, the discretization is determined by the resolution of the details. The tetrahedral (volume) mesh is constructed based on this triangular mesh.

Coupled to this inhomogeneous spatial discretization, an inhomogeneity is introduced in the time discretization through local time steps (as described in [19]) with a maximal ratio $\Delta t_{\min} / \Delta t_{\max}$ equal to 1/16. This increases significantly the efficiency of the computation, as the larger cells (in free-space) are updated 16 times less often than the small cells (around the feed). Local time-stepping algorithms are particularly advantageous for problems such as the present one, where the smaller cells in the mesh represents only a few percents of the total number of cells.

Figure 4 illustrates the return loss of the considered DRA, demonstrating a good agreement between the FVTD simulations and the measurements. Similarly, simulated and measured radiation patterns in the operation band are in good agreement, as shown for three frequencies in Fig. 5.

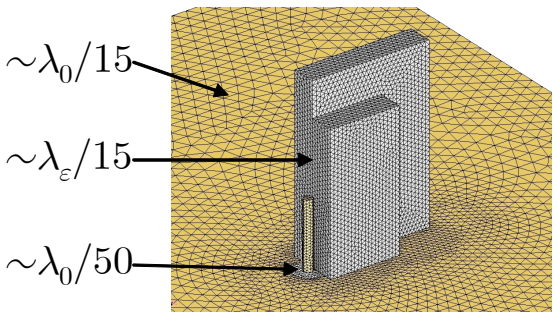

Fig. 3. Surface mesh of the two-step DRA, showing the different scales of the discretization. The tetrahedral mesh is built on the basis of this triangular surface mesh.

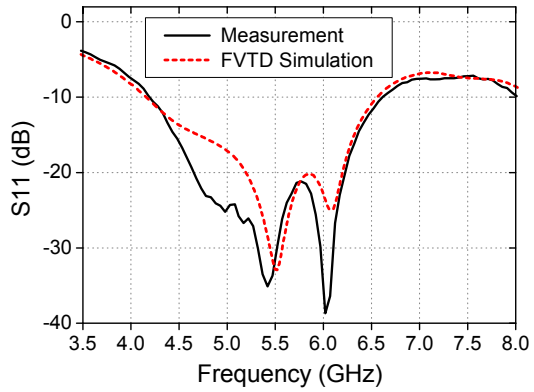

Fig. 4. Return loss of the two-step DRA showing an impedance bandwidth of 47%. A good agreement between simulation and measurement is achieved.

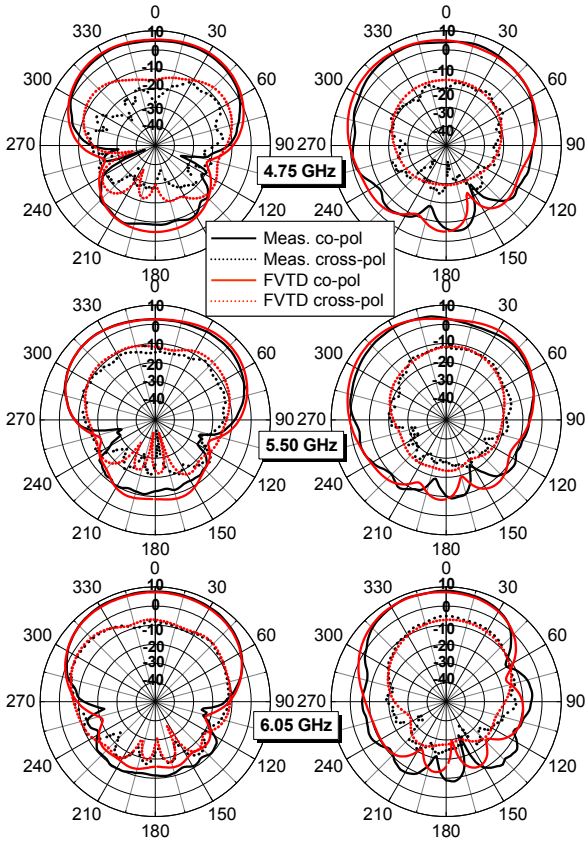

Fig. 5. Radiation patterns of the DRA at 3 frequencies. Left: E-plane, right: H-plane.

B. Evolutions of the DRA Shapes

The principle of operation of the two-step DRA is based on the excitation of three modes with similar characteristics. Conceptually, each of the modes can be attributed to a particular resonance in one of the slabs, although coupling to the second slab clearly affects the field distribution. Starting from this stepped structure, a semi-trapezoidal shape as shown in Fig. 6 can be interpreted as a continuous evolution from a multiple step DRA. This structure has been presented in [26], where the full design concept and the dimensions can be found. The return loss of the device, here simulated with FVTD, is compared in Fig. 7 to the measured data from [26] showing a reasonable agreement. A degradation is observed in the higher frequency range. It must be emphasized that fabrication and material tolerances are also introducing uncertainty in the comparison.

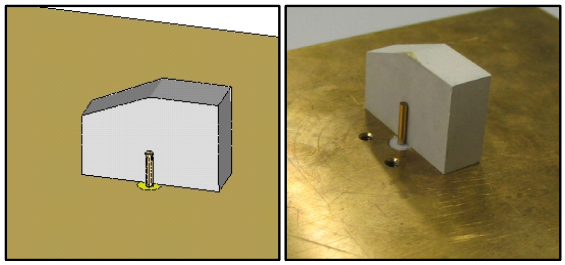

Fig. 6. Geometry of the semi-trapezoidal DRA. Left: simulation model, right: fabricated device.

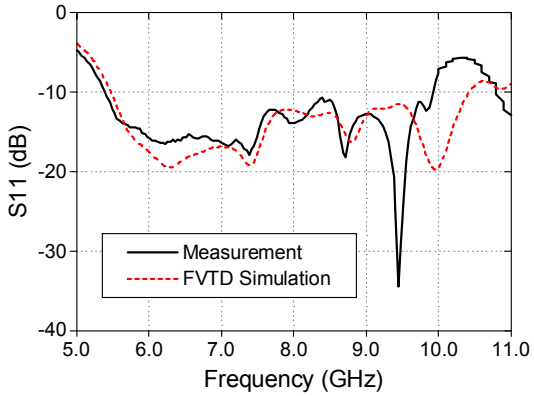

Fig. 7. Return loss of the semi-trapezoidal DRA, showing a measured 62 % impedance bandwidth.

The asymmetry in the design of the semi-trapezoidal DRA allows optimizing the impedance bandwidth. However, this asymmetry also affects the radiation pattern by skewing the broadside beam. Therefore, a further evolution of

the design symmetrises the structure, leading to the pyramidal DRA shown in Fig. 8 [27]. Again, the FVTD simulation of the device provides a return loss in good agreement with the measured data (Fig. 9). Compared to the asymmetric design, the pyramidal DRA is characterized by a slightly reduced bandwidth (48%), however with nicely behaved broadside patterns and polarization purity better than -20 dB.

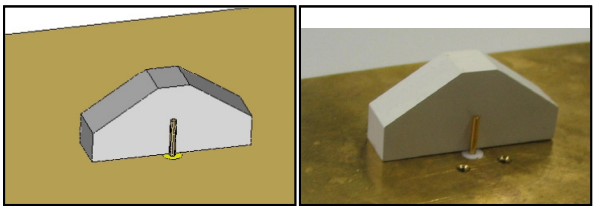

Fig. 8. Geometry of the pyramidal DRA. Left: simulation model, right: fabricated device.

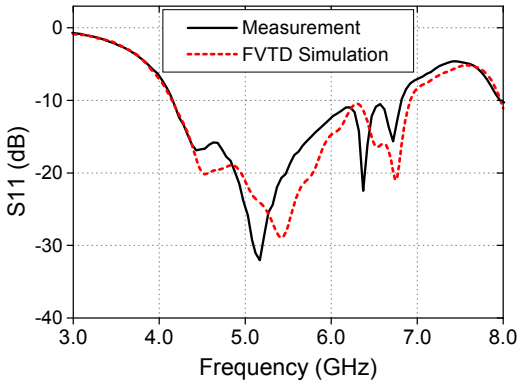

Fig. 9. Return loss of the semi-trapezoidal DRA, showing a measured 48% impedance bandwidth.

C. Mutual Coupling between Cylindrical DRAs

The last example considers the coupling between two simple probe-fed cylindrical DRAs on a common ground plane. The configuration is taken from [28]. In the present case, the computational domain takes the shape of an oblate ellipsoid in order to minimize the size of the computational domain while still including the full ground plane. A conformal PML is used as a finite-volume absorber to provide an accurate reflection-free domain truncation. The results plotted in Fig. 11 represent the S-parameters for the H-plane configuration of the two DRAs, with an inter-element spacing of 70 mm. Again, a very good agreement is observed between the FVTD simulation and the measurement. In this case, the transmission coefficients from the active antenna #1 to the passive antenna #2 is computed using the S-parameter extraction introduced in [7].

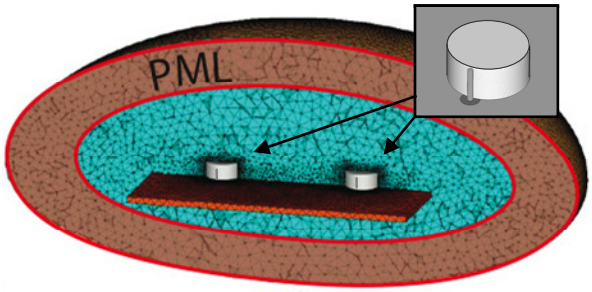

Fig. 10. Cut through the FVTD computational domain for the simulation of the H-plane coupling between two cylindrical DRA on a common ground plane. The inset show the geometry of a single DRA element.

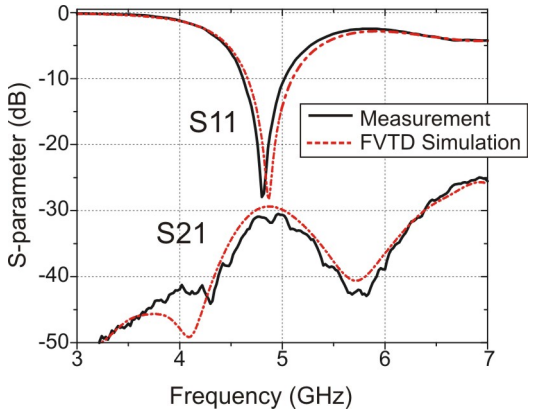

Fig. 11. Comparison of the measured and simulated S-parameters for the configuration of two DRAs shown in Fig. 10. S11: Return loss. S21: Transmission coefficient.

VI. CONCLUSION

Time-domain methods applied in conformal meshes such as the FVTD or the DG-TD methods can be expected to take an increasing role in the future of EM simulations, considering the miniaturization and growing complexity of devices. Multi-scale multi-domain schemes provide a promising approach to increase the efficiency and accuracy of this class of methods.

ACKNOWLEDGMENT

The authors would like to acknowledge the valuable support from H.-R. Benedickter, C. Maccio and M. Lanz.

REFERENCES

[1] A. Taflove and S.C. Hagness, "Computational Electrodynamics: The Finite-Difference Time-Domain Method", 3rd ed., Artech House, Norwood, MA, 2005.

[2] N.K. Madsen, R.W. Ziolkowski, "A three-dimensional modified finite volume technique for Maxwell's equations", *Electromagnetics*, Vol. 10, pp. 147–161, 1990.

[3] V. Shankar, A.H. Mohammadian, W.F. Hall, "A time-domain, finite-volume treatment for the Maxwell equations", *Electromagnetics*, Vol. 10, pp. 127–145, 1990.

[4] P. Bonnet, X. Ferrieres, B.L. Michielsen, P. Klotz, J.L. Roumiguières, "Finite-volume time domain method", Chapt. 9 in "Time domain electromagnetics", ed. by S.M. Rao, Academic Press, San Diego, 1999.

[5] K.S. Yee, J.S. Chen, "The finite-difference time-domain (FDTD) and the finite-volume time-domain (FVTD) method in solving Maxwell's equations," *IEEE Trans. Antennas Propagation*, Vol. 45, no. 3, pp. 354–363, 1997.

[6] B. van Leer, "Towards the ultimate conservative difference scheme. V. A second order sequel to Godunov's method", *J. Comp. Phys.*, Vol. 32, pp. 101–136, 1979.

[7] D. Baumann, C. Fumeaux, R. Vahldieck, "Field-based scattering-matrix extraction scheme for the FVTD method exploiting a flux-splitting algorithm", *IEEE Trans. Microwave Theory Techniques* Vol. 53, no. 11, pp. 3595–3605, 2005.

[8] P. Bonnet, X. Ferrières, F. Issac, F. Paladian, J. Grando, J.C. Alliot, J. Fontaine, "Numerical modeling of scattering problems using a time domain finite volume method", *J. of Electromagnetic Waves and Appl.*, vol. 11, pp. 1165–1189, 1997.

[9] X. Ferrières, J.P. Parmantier, S. Bertuol, A.R. Ruddle, "Application of a hybrid finite difference/Finite Volume method to solve an automotive EMC problem", *IEEE Trans. Electromagnetic Compatibility*, vol. 46 , pp. 624–634, 2004.

[10] Y. Shi, C.-H. Liang, "The Finite-Volume Time-Domain algorithm using least square method in solving Maxwell's equations", *J. Comp. Phys*, vol. 226, pp. 1444-1457, 2007.

[11] C. Fumeaux, D. Baumann, R. Vahldieck, "Finite-Volume Time-Domain analysis of a cavity-backed Archimedean spiral antenna", *IEEE Trans. Antennas Propagation*, Vol. 54, no. 3, pp. 844–851, March 2006.

[12] D. Firsov, C. Kaye, J. LoVetri, "FVTD thin-wire modelling of a microwave tomography system", *Proc. of the 24th international ACES Conference*, Niagara Falls, Canada, March 30-April 4, 2008.

[13] J.S. Shang, M. Wagner, Y. Pan, D.C. Blake, "Strategies for Adopting FVTD on Multicomputers", *Computing in Science and Engineering*, Vol. 2, no. 1, pp. 10–21, 2000.

[14] C. Fumeaux, K. Sankaran, R. Vahldieck, "Spherical perfectly matched absorber for finite-volume 3-D domain truncation", *IEEE Trans. Microwave Theory Techniques*, Vol. 55, no. 12, pp. 2773–2781, 2007.

[15] C. Bommaraju, W. Ackermann, T. Weiland, "Finite Volume Time Domain method on TET & HEX meshes", *Proc. 7th Workshop Comp. Electromagnetics Time-Domain (CEM-TD 2007)*, Perugia, Italy, Oct. 15-17, 2007.

[16] D. Firsov, J. LoVetri, I. Jeffrey, V. Okhmatovski, C. Gilmore, W. Chamma, "High-order FVTD on unstructured grids using an object-oriented computational engine", *ACES Journal*, Vol. 22, pp. 71–82, 2007.

[17] J.S. Hesthaven and T. Warburton, "Nodal Discontinuous Galerkin methods: algorithms, analysis, and applications", Springer Texts in Applied Mathematics Vol. 54, Springer Verlag, New York, 2008.

[18] E.T. Chung, B. Engquist, "Optimal Discontinuous Galerkin methods for wave propagation", *SIAM J. Numerical Analysis*, Vol. 44, no.5, pp. 2131–2158, 2006.

[19] C. Fumeaux, D. Baumann, P. Leuchtmann, R. Vahldieck, "A generalized local time-step scheme for efficient FVTD simulations in strongly inhomogeneous meshes", *IEEE Trans. Microwave Theory Techniques* Vol. 52, no. 3, pp. 1067–1076, 2004.

[20] S. Piperno, "Symplectic local time-stepping in non-dissipative DGTD methods applied to wave propagation problems", *ESAIM: Mathematical Modelling and Numerical Analysis*, Vol. 40, No 5, pp. 815–841, 2006.

[21] A. Catella, V. Dolean, L. Fezoui, S. Lanteri, "Efficient time integration strategies for high order discontinuous Galerkin time domain methods", *Proc. of the 24th international ACES Conference*, Niagara Falls, Canada, March 30-April 4, 2008.

[22] D.K. Firsov, J. LoVetri, "FVTD-integral equation hybrid for Maxwell's equations", *Int. J. Numer. Model.*, Vol. 21, pp. 29–42, 2007.

[23] S. Schnepp, E. Gjonaj, T. Weiland, "An hp-adaptive Discontinuous Galerkin method in time Domain applied to the simulation of highly localized current sources", *Proc. of the 24th international ACES Conference*, Niagara Falls, Canada, March 30-April 4, 2008.

[24] S. A. Long, M. W. McAllister and L. C. Shen, "The resonant cylindrical dielectric cavity antenna," *IEEE Trans. Antennas Propagation*, Vol. 31, no. 3, pp. 406–412, May 1983.

[25] G. Almpanis, C. Fumeaux, R. Vahldieck, "Two-step rectangular dielectric resonator antenna", *First European Conf. Antennas and Propagation (EuCAP)*, Nice, France, 6–10 November 2006.

[26] G. Almpanis, C. Fumeaux, R. Vahldieck, "Semi-trapezoidal dielectric resonator antenna for wideband applications", *IEEE Antennas Propagation Soc. Int. Symp. (AP-S*), Honolulu HI, pp. 4877–4880, June 10-15, 2007.

[27] G. Almpanis, C. Fumeaux, R. Vahldieck, "Pyramidal dielectric resonator antennas for wideband applications", *2nd European Conf. Antennas and Propagation (EuCAP)*, Edinburgh, UK, 11-16 November, 2007.

[28] C. Fumeaux, G. Almpanis, K. Sankaran, D. Baumann, R. Vahldieck, "Finite-Volume Time-Domain modeling of the mutual coupling between dielectric resonator antennas in array configurations", *2nd European Conf. Antennas and Propagation (EuCAP)*, Edinburgh, UK, 11-16 November, 2007.